Influence of Welding on the Dissolution of API- 5 L X60 in Simulated Soil Solution- Corrosion Protection by Phosphoric Compound- DFT Calculations

Lahdiri, Ouahiba; Kellou-Kerkouche, Farida*+; Idir, Brahim•

USTHB, Laboratory of Electrochemistry-Corrosion, Metallurgy and Mineral Chemistry, Faculty of Chemistry El-Alia Bab-Ezzouar Algiers, ALGERIA

ABSTRACT: *The present work aims to examine the susceptibility to soil corrosion of base metal (BM) and heat affected zone (HAZ) of API L5 X60 steel pipeline, and to assess the ability of Di-(2-ethylhexyl) phosphoric acid (D2EHPA) to inhibit the corrosion of the two samples. An overview of the literature reported almost no studies related to the corrosion inhibition of pipeline in soil solutions. The experiments were carried out in a simulated soil solution (NS3) using electrochemical methods, a thermodynamic approach, and surface analysis. The results demonstrated that D2EHPA is a potent inhibitor for both steels in the soil solution. Indeed, its efficiency increased with the increase of its concentration, exceeding 98 % at the optimal concentration, even for HAZ which is less resistant to corrosion than BM, due to the coarsening of α-ferrite grains. Polarization curves showed that D2EHPA acts as an anodic-type inhibitor, and the calculated standard free adsorption energy values deduced by Langmuir isotherm indicated that the phosphoric compound adsorbs via electrostatic and chemical bindings. The stability of the adsorbed D2EHPA layer, on both the surfaces of BM and HAZ that were immersed in the inhibitive solution for 168 h, has been proven by EIS studies. Moreover, the effective adsorption of D2EHPA at the steel/SN3 interface is clearly highlighted by Scanning Electron Microscopy (SEM) and FT-IR spectra. Theoretical DFT calculations were also performed to determine some electronic properties of the studied molecule, and to find a correlation between the inhibitive effect and the electronic structure of the neutral form and the deprotonated form of D2EHPA.*

KEYWORDS: *Soil corrosion; API-5L X60; Corrosion inhibition; EIS; DFT calculations.*

INTRODUCTION

The consumption of gas and oil increases day by day, and pipelines are the preferred alternative for transporting large volumes of crude oil, natural gas, and petroleum products over long distances from the production sites to the consumers. Thus, it is necessary to maintain the pipeline network by protecting it against the various problems it may face, particularly corrosion. Indeed, corrosion largely contributes to the reduction of

* *To whom correspondence should be addressed*
+ E-mail: fkerkouche9@gmail.com
● *Other Address: Research Center in Industrial Technologies (CRTI), Cheraga Algiers, ALGERIA*
1021-9986/2023/4/1356-1375 20/$/7.00

the resistance of the pipes and, consequently, their maximum operating pressure [1].

Carbon steels like API-5L steels are the most used materials in pipeline construction due to their low cost, the mastery of their development techniques and their production, and their mechanical properties such as strength, toughness, and good weldability.

One of the most important factors in the safe operation of pipelines lies in the properties of weldment [1] which creates three zones: the Base Metal (BM), the Weld Metal (WM), and the Heat Affected Zone (HAZ). In the aggressive media, these regions are susceptible to different types of corrosion [2-4]. For example, minor differences in the composition and microstructure between HAZ and BM can result in an electrochemical galvanic effect, affecting the corrosion resistance of the pipeline [5]. Indeed, it has been found that the corrosion susceptibility of HAZ is enhanced due to phase changes during the welding process as a result of the extreme temperature gradient [6-8].

The external surface of buried pipelines is exposed to soil corrosion, which is a complex phenomenon representing an important factor in pipeline failure. It has been reported that the aggressiveness of soil depends not only on its mineralogical character but also on its moisture content, pH, soluble ionic species, resistivity, and its degree of aeration [7].

During the last decades, several works have been dedicated to the soil corrosion of pipelines [8-12]. *Durr C.L. et al*. [9] focused their research on the evaluation of the existing techniques used for assessing the soil corrosion of steel pipelines. They found that certain variables are mandatory to describe the corrosivity of a soil. On the other hand, the effect of soil moisture content on the corrosion behavior of X60 steel in three types of soil was examined in ambient temperature [10]. The results showed an increase of corrosion rate with increasing soil moisture content up to a maximum value of 10% and a decrease for higher values. Other authors [11] indicated that the API 5L X52 steel is more resistant to corrosion in aqueous extracts of soil than in synthetic soil solutions. Moreover, a correlation between soil resistivity and corrosion growth of API 5L X70 steel has been established by *Lim K.S. et al*. [12]. They affirmed that soil resistivity is an indicator used to test the aggressiveness of soil. Indeed, they found a negative logarithmic relationship between soil resistivity and soil corrosiveness *via* regression analysis.

Among all the procedures used for protecting mild steels against corrosion, the use of corrosion inhibitors is one of the most practical methods, given that it presents economic and environmental advantages, great efficiency, and high applicability [13-15]. In recent decades, a variety of inorganic compounds such as sodium molybdate [16] and organic compounds such as hexamethylenetetramine [17] were added to aggressive solutions to prevent the corrosion of ferrous materials in various corrosive environments. Organic inhibitors can adsorb onto the metal surface through heteroatoms (nitrogen, oxygen, sulphur, and phosphorus), multiple bonds, or aromatic rings, decreasing the corrosion rate by blocking the active sites [18-21]. The inhibitor adsorption is influenced by molecular structure, molecular size, molecular weight, electron density of the heteroatoms, charge of the metal surface, and the nature of the electrolyte [22-24]. Many compounds have been used in various industries as effective corrosion inhibitors (especially in the oil industry), however some of them are toxic and harmful for the environment [25,26]. Indeed, toxic inhibitors, which include aromatic and nitrogen containing heterocyclic compounds, are used in pickling processes and in the oil and gas industry [27]. Nowadays, phosphonates are widely applied as corrosion inhibitors in cooling water treatments because of their relatively good performance and attractive environmental characteristics. *Karthik et al*. [28] claimed that several phosphonic acids were used as corrosion inhibitors, given their stability and their ability to form complexes with metal cations such as Zn^{2+}ions. These complexes adsorb on the anodic sites of the metal surface and control the anodic process. Di-(2-ethylhexyl) phosphoric acid is generally used as an extractant of metals, and at pH higher than 4 its dissolution increases significantly due to its deprotonation and the domination of its negatively charged species [29]. Thus, the latter react with the metal cations by forming soluble complexes that eventually precipitate on the metallic surface to form a protective film.

In this paper, we have examined the susceptibility of the base metal (BM) and the heat affected zone (HAZ) of API L5 X60 pipeline steel to soil corrosion and their protection against corrosion. For this purpose, we used a simulated soil solution (NS3) as an aggressive medium and Di-(2-ethylhexyl) phosphoric acid as a corrosion inhibitor. In our knowledge, the corrosion inhibition of the studied samples has never been examined in this type of environment and D2EHPA has never been used as a corrosion inhibitor. This

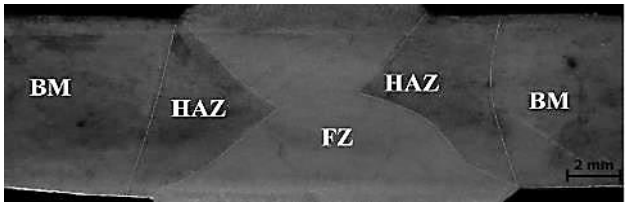

Fig. 1: The macromorphology of the three zones of welded X60 steel by SAW.

investigation was conducted using electrochemical methods, a thermodynamic approach and surface analysis. It was supplemented by a theoretical study using DFT calculations [30-32] to explain the obtained experimental results. The quantum calculations describe the structural nature of the inhibitor molecule, which offers further insight into the mechanism of the inhibitory action of D2EHPA in the corrosion process.

EXPERIMENTAL SECTION

Materials

"Algerian Metal Tubes" (ALTUMET) supplied the two ferrous materials used in this study: base metal (BM) of API 5L - X60 and heat affected zone (HAZ), which were extruded from two different regions of a longitudinal weld joint. This was obtained using submerged arc welding (SAW). In the SAW process, using a filler metal with A5.23/A5 23M: EA2 AWS specification, both the weld electrode and BM were melted beneath a layer of flux. This layer protects the weld metal against the harmful action of ambient air, consisting of oxygen, nitrogen, and humidity. It is also used to concentrate the heat into the joint. The molten flux rises through the weld pool, deoxidizing and cleaning the molten metal. The macromorphology of the three zones appearing during the welding is presented in Fig. 1, they are: The Base Metal (BM), the Fusion Zone (FZ), and the Heat Affected Zone (HAZ). In this study, only BM and HAZ are considered.

These materials have been used in the as-received state, with no further heat treatment. The chemical compositions of API 5L X60 steel and the filler metal were analyzed by Optical Emission Spectrometer (foundry-master pro) and are given respectively in Table 1 and Table 2. The two cylindrical samples, which were used as working electrodes for all the electrochemical tests, were cut from the longitudinal weld joint and connected to wires using conductive copper then

Table 1: Chemical composition of the API 5L X60 pipeline steel (wt %).

Fe	C	Si	Mn	P	S
98.1	0.0508	0.239	1.30	0.0018	0.0018
Cr	Cu	Nb	Co	Ni	
0.0376	0.0159	0.0404	<0.0005	0.0202	

Table 2: Chemical composition of the filler metal (wt %).

C	Si	Mn	P	S	Cr	Cu
0.100	0.15	1.06	0.006	0.001	0.04	0.05
Mo	Co	V	Al	Ni	N	
0.51	0.006	<0.01	0.001	0.07	0.004	

Table 3: Chemical composition of the simulated soil solution (NS3) in g/L.

NS_i	KCl	$NaHCO_3$	$CaCl_2.2H_2O$	$MgSO_4.7H_2O$
NS_1	0.149	0.504	0.159	0.106
NS_2	0.142	1.031	0.073	0.254
NS_3	0.037	0.559	0.008	0.089
NS_4	0.122	0.483	0.181	0.131

embedded in hard cold-curing epoxy resin. Before each experiment, the cross-section of the working electrodes (0.382 cm^2) was sequentially wet-ground with 320, 600, and 1200 grit silicon carbide emery papers, degreased in acetone, rinsed with distilled water, dried and transferred in a glass cell filled with 100 ml of the test solution.

Aggressive and inhibitive solutions

The chemical composition of the soil shows that the main electrolytes contained in the soil of the pipe are variable proportions of carbonates, bicarbonates, chloride and sulphate depending on the pipe sites [33]. A simulated ground water solution, called NS3 with pH=8.3, was employed as the corrosive environment in the present study. Its chemical composition is presented in Table 3.

The corrosion inhibitor Di-(2-ethylexyl) phosphoric acid (D2EHPA) was purchased from Fluka AG, CH-9470 Buch. It was available in an aqueous solution of 50 % active acid content. The molecular structure of this compound is shown in Fig. 2. D2EHPA was added to freshly prepared NS3 in the concentration range of (0.04-0.16 mM) with an increment of 0.04 mM. It complies with standards and regulations concerning toxicity and environment. Indeed, its maximum concentration used in this study is 0.16 mM, which is a low concentration.

Solutions were continuously stirred during the electrochemical tests occurring at 293 K.

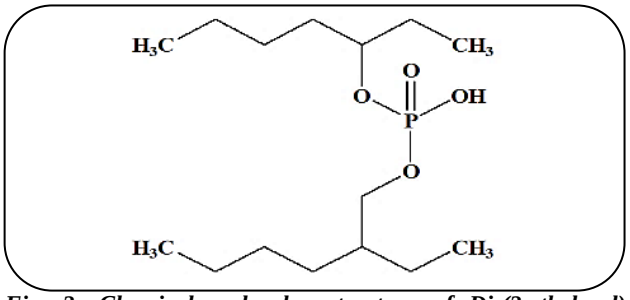

Fig. 2: Chemical molecular structure of Di-(2-ethylexyl) phosphoric acid (D2EHPA)

Electrochemical techniques

The electrochemical measurements were performed in a conventional three electrodes cell. The samples (BM and HAZ) were used as working electrodes (WE); platinum wire and saturated calomel (SCE) were used as auxiliary and reference electrodes, respectively. Potentiodynamic polarization curves were carried out using a computer-controlled Potentiostat PGP 201 and Voltamaster 4 software was employed for assessing the experimental data. Before each electrochemical test, the open circuit potential (OCP) was monitored for 1800 s to establish a steady state followed by the plot of potentiodynamic polarization curves in the cathodic-anodic direction, at the scan rate of 2 mV/s. The electrochemical impedance spectroscopy (EIS) technique was implemented with Solartron Analytical 1287 Potentiostat-Galvanostat and a 1260 Impedance/game phase Analyzer. EIS diagrams were carried out at the OCP, in the frequency range from 0.01 Hz to 100 kHz, with 10 points per decade, using a 10 mV peak-to-peak voltage excitation. The diagrams analysis was done by ZPlot software and the impedance data were fitted with Zview software using the equivalent circuit models. All the electrochemical tests were carried out three times to confirm the reasonable reproducibility of the results, without and with D2EHPA at various concentrations.

Characterization and analysis of metallic materials

The microstructures of BM and HAZ, immersed during 168 h in the soil solution without and with D2EHPA, were observed by Scanning Electron Microscope (SEM) using ESEM Philips XL30 with tungsten filament. This was obtained by applying an acceleration potential of 20 kV, and by an optical microscope NIKON Eclipse LV 100 ND, after mirror polishing and etching their surface with a nital solution (96% ethanol+4% nitric acid) for 15 s. Infrared spectra of pure D2EHPA and the adsorbed layer on BM and HAZ were recorded with FT-IR/ATR spectrometer (Alpha Bruker) in the range of (4000-400 cm^{-1}) surface, after 168 h of immersion in NS3 solution in presence of D2EHPA at 0.16 mM.

Computational method

The quantum chemical calculations were performed using Kohn–Sham's Density Functional Theory (DFT) subjected to the gradient-corrected hybrid density functional B3LYP [34-36]. This functional is a combination of the Beck's three parameters non-local exchange potential with the non-local correlation functional of *Lee et al*. [37] and *B. Miehlch et al*. [38]. A full geometry optimization of D2EHPA and $D2EHPA^{-}$was performed in water phase using this functional and the 6-31G (d, p) [39,40] basis set as implemented by Spartan 10.0 package [41]. The vibrational frequencies were computed to ensure that the stationary point is minimal.

Some DFT descriptors such as the dipole moment (μ), the energy of the highest occupied molecular orbital (E_{HOMO}) and the energy of the lowest unoccupied molecular orbital (E_{LUMO}), were determined. Hardness (η), global electrophilicity (ω) [42,43], global nucleophilicity (ε) and absolute electronegativity (χ) [44], were deduced from the *Eqs.* (1) and (2):

$$\chi = \frac{1}{2}(I + A) \quad (1)$$

Where: Ionization potential $I = -E_{HOMO}$ and electron affinity of the molecule $A = -E_{LUMO}$

$$\eta = \frac{1}{2}(I - A) \quad (2)$$

Global electrophilicity index ω introduced by *Parr at al*. [45] can be calculated from *Eq.* (3):

$$\omega = \frac{\chi^2}{2\eta} \quad (3)$$

Nucleophilicity (ε) is the inverse of electrophilicity ($1/\omega$) [46]. Thus, a good nucleophile is characterized by a high value of (ε) and a good electrophile is characterized by a high value of (ω). During the interaction between the inhibitor and the metal surface by chemical bonds, the fraction of the electrons transferred from D2EHPA and $D2EHPA^{-}$ to iron (ΔN) was calculated with the following *Eq.* (4) [47]:

$$\Delta N = \frac{\chi_{Fe} - \chi_{inh}}{2(\eta_{Fe} + \eta_{inh})} \quad (4)$$

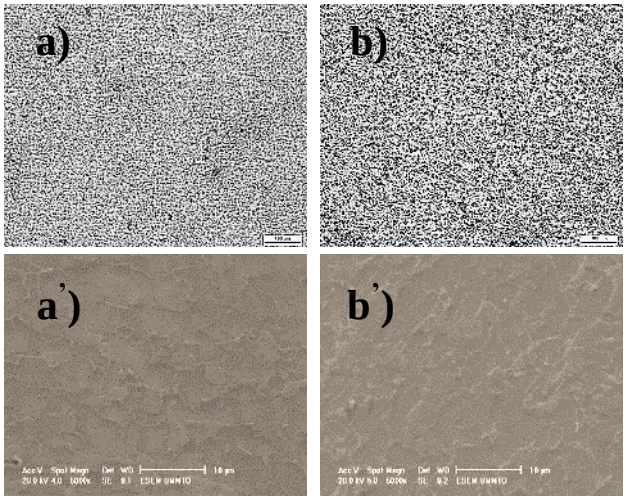

Fig. 3: Optical micrographs of a) BM and b) HAZ and SEM micrographs of a') BM and b') HAZ.

Where χ_{Fe}, χ_{inh}, η_{Fe}, η_{inh} are electronegativities and hardness values of iron and inhibitor molecule, respectively. Theoretical values of χ_{Fe} and η_{Fe} are 7 eV and 0 eV, respectively [48].

RESULTS AND DISCUSSION

Surface observation

The optical and SEM micrographs obtained after etching the surface metal with nital solution are depicted in Fig. 3.

We can clearly see that the microstructure of base metal (Fig. 3 (a)) consists of two phases: a predominant bright ferritic phase, represented by acicular grains, which is an interstitial solid solution of a small amount of carbon dissolved in α-Fe with a bcc crystal structure, and a small amount of dark pearlitic phase composed of an alternation of ferrite and cementite (Fe_3C) phases [49]. As for the microstructure of the heat affected zone (Fig. 3 (b)), it is represented by larger grains of acicular ferrite with a small amount of pearlite and probably bainitic lath type regions [16]. It has been documented that as the considered zone moves from the weld region, the peak temperature during welding is lower, inducing relatively coarse grains of ferrite [16]. The same phenomenon occurred for the studied HAZ sample during the welding process, which is followed by a slow air cooling.

Electrochemical and thermodynamic studies

Spontaneous behavior of materials in the soil solution at 293 K

The free potential or OCP variation over immersion time describes the spontaneous behavior of materials in

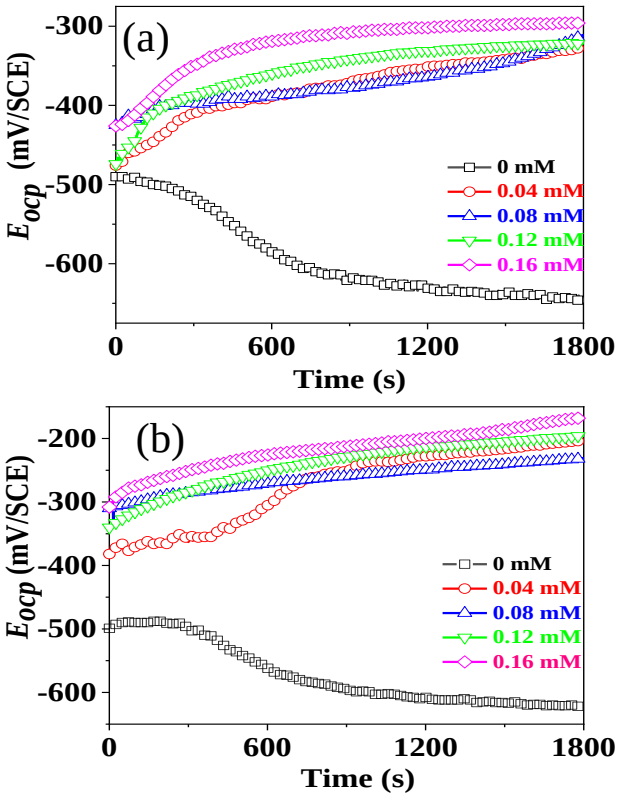

Fig. 4: OCP variation against immersion time for a) BM and b) HAZ in NS3 solution at various concentrations of D2EHPA at 293 K.

electrolytic solutions. Fig. 4 illustrates the free potential evolution of BM and HAZ X60 pipeline steel in NS3 simulated soil solution, without and with various concentrations of D2EHPA at 293K for 1800 s. It is obvious that in the early stage of immersion, the OCP of the two samples, in the blank, solution shifts rapidly to the cathodic values, and its variation reaches 155 mV for BM and 126 mV for HAZ X60 after 1800 s of immersion. This phenomenon reflects the activation of the two ferrous alloys in the studied aggressive solution. Thus the corrosion rate becomes dependent on the diffusion rate of oxygen in soil water, and the whole corrosion reaction falls under cathodic control, corresponding to oxygen reduction ($O_2 + 2H_2O + 4é \rightarrow 4OH^-$) which predominates in near neutral or alkaline solutions. *De Sena et al*. [50] described the same behavior for the API 5L X65 in a soil solution and attested that the OCP recorded in a deaerated solution is approximatively 50 mV more negative than in the aerated one. Other studies [10, 51] have reported a potential shift of about 300 mV vs. SCE towards more cathodic values for API 5L, X46, X60, and X80 steels immersed

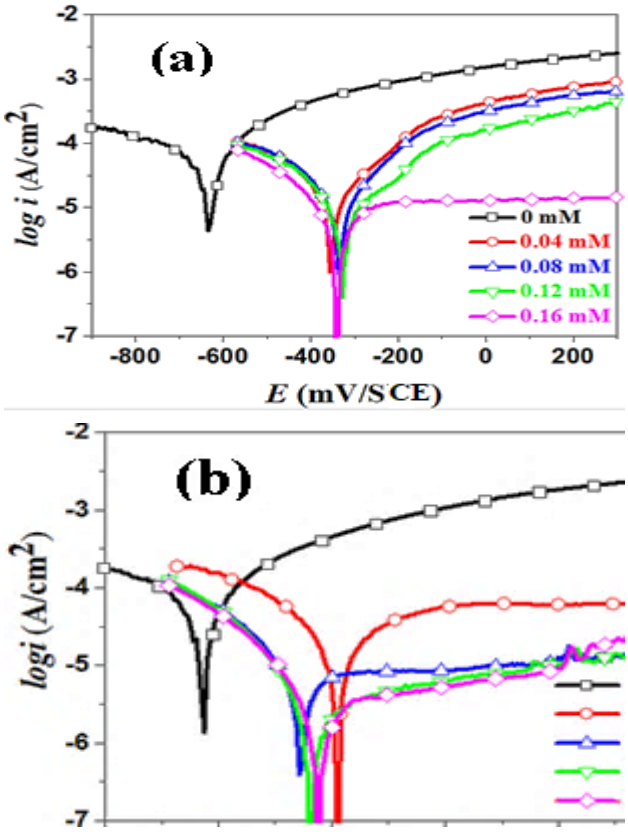

Fig. 5: Potentiodynamic polarization curves at different concentration of D2EHPA for a) BM and b) HAZ in NS3 solution at 293 K.

soil solution, purged with pure N_2. Consequently, the oxygen influence is evident in the soil solutions.

In contrast, the OCP of the two samples immersed in the simulated soil solution, with various concentrations of D2EHPA, shifted rapidly to the anodic values and its variation reached 349 mV and 427 mV for BM and HAZ, respectively, at 0.16 mM of phosphoric compound, after 1800 s of immersion. Therefore, the ennoblement of the OCP results from the formation of a barrier layer, made up of D2EHPA molecules, which isolate the metal surface from the aggressiveness of the soil solution.

It should be noted that the D2EHPA effect is more pronounced on the spontaneous behavior of HAZ. This phenomenon could be related to the difference in morphology of the microstructures of the two samples which will be discussed below.

Potentiodynamic polarization curves at 293 K

The electrochemical behavior of BM and HAZ immersed in NS3 solution at 293 K was analyzed by means of polarization curves which are depicted in Fig. 5 (a,b). Tafel parameters are listed in Table 4. From the latter, we can see that the current density (i_{corr}) of HAZ is higher than that of BM, while the values of their corrosion potential are very close. Thus HAZ sample is more susceptible to soil corrosion than BM sample, in these experimental conditions. The same results were found for BM and HAZ regions of API 5L-X52 steel immersed in 3.5 % NaCl [16] and for welded X80 pipeline steel zones in a simulated soil solution [1]. It has been reported that the corrosion is related to the grain size and that the grain boundaries are preserved after the corrosive attack [1]. From this observation, it can be suggested that the cathodes are represented by the carbides (Fe_3C) of the pearlite phase, which precipitated at grain boundaries, while the ferrite phase plays the role of anodes [52]. Thus, the larger the anodic sites, the more interfacial contacts and the more micro-corrosion cells will form, resulting in a more severe metal attack [53].

The polarization curves illustrated in Fig. 5 (a,b) are plotted for BM and HAZ immersed in NS3 solution in the absence and in presence of various concentrations of D2EHPA at 293 K.

Obviously, the general shape of the cathodic polarization curves of BM and HAZ steels in the simulated soil solution (NS3) in the presence of Di (2-ethylhexyl) phosphoric acid remains unchanged. Therefore, the addition of D2EHPA to the corrosive solution does not modify the mechanism of the oxygen reduction process. Since the cathodic portion curves of the two samples with and without D2EHPA are characterized by parallel Tafel lines, and then the cathodic process is under activation control [13]. This means that the phosphoric compound does not modify the mechanism of the oxygen reduction reaction. In contrast, the elementary anodic curves profile of the two samples, in presence of D2EHPA, recorded some changes revealing a quasi-plateau in current at 0.16 mM of inhibitor, especially for BM. This phenomenon might be related to the modification of the iron anodic dissolution process ($Fe \rightarrow Fe^{2+} + 2é$), due to the inhibitor molecules adsorption onto the active sites of BM and HAZ. This has also resulted in a very significant decrease in the anodic current densities, especially at the optimum D2EHPA concentration for BM and at all the concentrations of the inhibitor for HAZ. As it appears in the polarization curves (Fig. 5), the corrosion potential has undergone

Table 4: Tafel electro-kinetic parameters for BM and HAZ X60 pipeline steel in NS3 simulated soil solution with various concentrations of D2EHPA at 293 K

Samples	C mM	E_{cor} mV_{SCE}	i_{cor} µA/cm²	b_a mV/dec	-b_c mV/dec	IE%
BM	0	-635.1	32.84	131.8	197.1	/
	0.04	-356.5	13.28	178.3	168.3	59.56
	0.08	-338.0	8.08	126.7	122.8	75.39
	0.12	-331.1	5.86	160.5	116.4	82.21
	0.16	-341.9	4.24	207.1	122.8	87.80
HAZ	0	-630.5	46.50	167.5	221.9	/
	0.04	-393.5	13.72	214.0	146.0	70.49
	0.08	-257.2	4.21	263.1	214.0	90.09
	0.12	-322.3	2.90	169.8	107.7	93.76
	0.16	-236.2	2.28	214.9	105	95.09

notable shift towards more anodic values. These results indicate that Di (2-ethylhexyl) phosphoric acid acts as an inhibitor with predominant control of the anodic reaction for both materials. It seems that the inhibitive molecules adsorb better onto the HAZ surface, thus on the anodic sites of HAZ represented by the ferritic phase.

The electrochemical kinetic parameters, in presence of D2EHPA, were determined from polarization curves (Table 4) by extrapolating the linear Tafel regions to the corrosion potential: the corrosion potential (E_{cor}), the corrosion current density (i_{cor}), cathodic Tafel slope (b_c), anodic Tafel slope (b_a), as well as the percentage inhibition efficiency IE (%) defined by *Eq.* (5):

$$IE\ (\%) = \frac{i_o - i_{corr(inh)}}{i_o} \times 100 \qquad (5)$$

Where: i_o and $i_{corr(inh)}$ are the corrosion current density values without and with the inhibitor, respectively.

A significant anodic shift in corrosion potential (E_{cor}) has been recorded, for both metals, in the presence of various concentrations of D2EHPA, attesting that the inhibitor is of anodic type [24,54,55]. Moreover, since the anodic Tafel slope (ba) and the cathodic Tafel slope (bc) values vary with the addition of D2EHPA, the inhibitor controls both the anodic and cathodic reactions [56]. The data of Table 4 showed that corrosion current densities decreased with the increase of D2EHPA concentration until 0.16 mM, which induced a maximum inhibition efficiency of 87.80% for BM and 95.09% for HAZ. Note that D2EHPA is more efficient in the case of HAZ and its addition to the soil solution, in small amount such as 0.08 mM, has induced high protection (90.09%), this could be attributed to its good adsorption onto the anodic sites represented by the coarse-grained ferritic phase in the HAZ microstructure.

Electrochemical impedance spectroscopy study

Fig. 6 (a, b) displays the Nyquist plots for BM and HAZ steels obtained at the OCP after immersion in the NS3 soil solution for 1800 s without and with D2EHPA. It is noted that all the Nyquist diagrams of BM (Fig. 6 (a)) and HAZ (Fig. 6 (b)) exhibit only one time constant represented by a single depressed half circle over the studied frequency range, suggesting a charge transfer control for the corrosion process of both steels [23]. Therefore, the mechanism of the corrosion process was not affected by the addition of the phosphoric compound to the soil solution.

The imperfect semicircle may be attributed to surface roughness, frequency dispersion, as well as heterogeneity of the surface of pipeline steels [57,58]. It is evident that the impedance response of the two samples has changed considerably after the addition of D2EHPA to the aggressive soil solution. Indeed, the diameters of the capacitive arcs in the presence of the inhibitor are larger than those observed in its absence and expand further as its concentration increases. This phenomenon could be attributed to the adsorption of the inhibitor onto BM and HAZ surfaces by blocking its active sites, inducing an improvement of corrosion protection of the two ferrous materials in the inhibitive soil solution [59, 60].

The Bode diagrams represented by phase angle plots are depicted in Fig. 6 (a', b'), they supplement the information provided by the Nyquist diagrams when the corrosion processes are very complex.

The plots of BM (Fig. 6 (a')) and HAZ (Fig. 6 (b')) show only one peak; this confirms the existence of a single time constant describing the metal/surface interface [57. It is evident that the angle phase values at medium frequencies have changed significantly towards more negative values, and the phase angle curve widens as the D2EHPA concentration increases, which attests to the strengthening of the adsorption of the inhibitor on the metal surface [61], after the addition of D2EHPA to the corrosive soil solution.

All the impedance diagrams were fitted accurately with a good chi-squared (χ^2) in the order of 10^{-3}, using the Randles electrical equivalent circuit (R_S (R_{ct}//CPE)) as illustrated in Fig. 7. In this equivalent circuit, R_s is the electrolyte resistance, R_{ct} represents the charge transfer

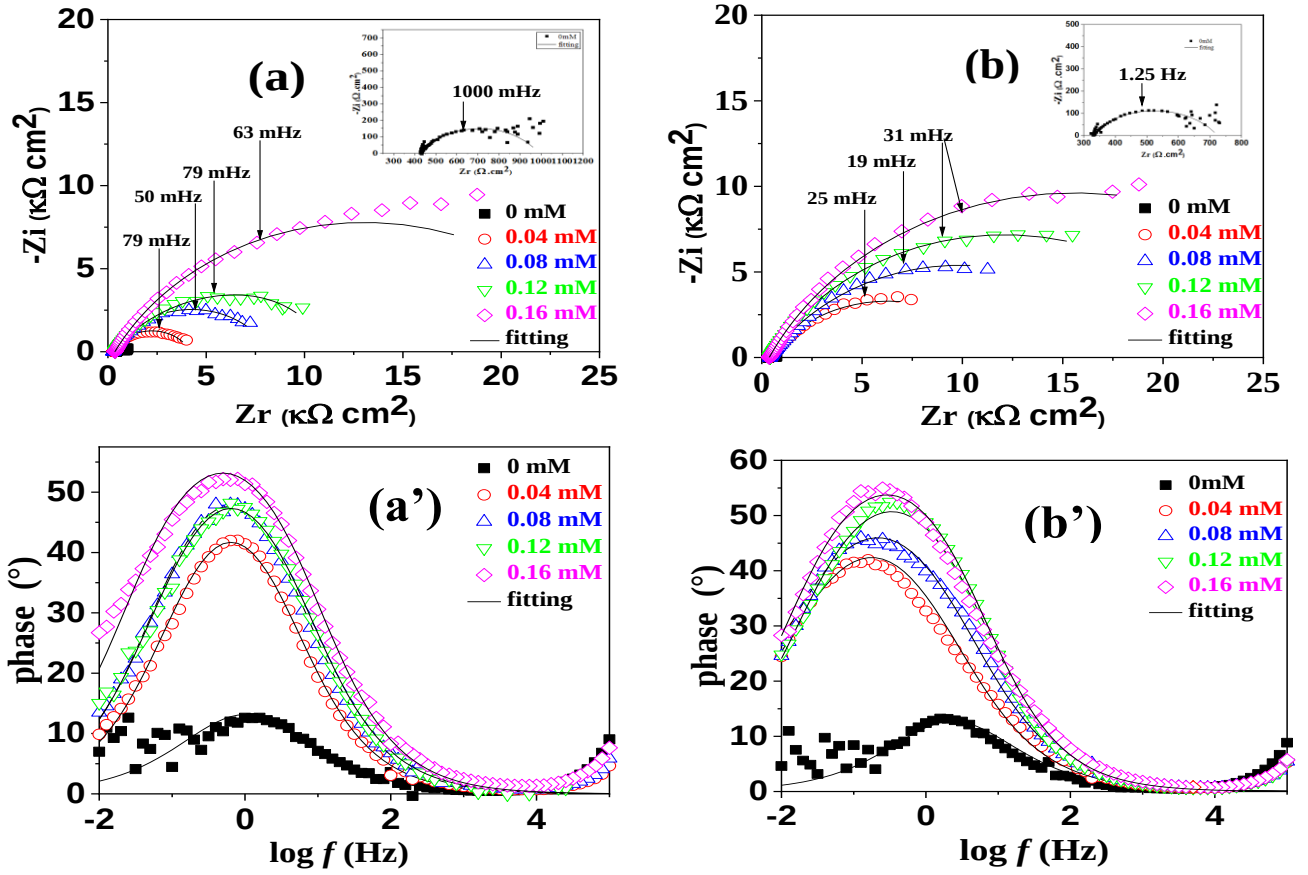

Fig. 6: Nyquist plots for a) BM and b) HAZ and Bode plots of a') M and b') HAZ in soil solution at various concentrations of the used inhibitor at 293 K.

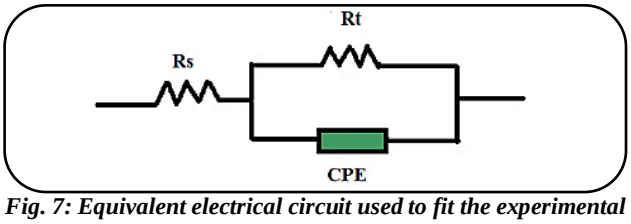

Fig. 7: Equivalent electrical circuit used to fit the experimental EIS data

resistance related to the spontaneous corrosion process and CPE is the constant phase element, reflecting the non-ideality of the double layer capacitance (C_{dl}). The CPE behavior is generally believed to originate from the distribution in the current density along the electrode surface, as a result of electrode roughness and inhomogeneity. This can be inferred from the analogy with the behavior of porous electrodes [62].

The Constant Phase Element (CPE) is introduced to simulate the non-ideal capacitive behavior of ferrous material solution interface, as it was reported by previous studies [63, 64] and its impedance is defined by the (Eq. (6)) [65]:

$$Z_{CPE} = \frac{1}{Y_0(j\omega)^n} \quad (6)$$

where: ω is the angular frequency ($\omega = 2\pi f$, f represents the AC frequency in Hz) and j is the imaginary unit ($j^2 = -1$). Y_0 is the CPE constant and n is the CPE exponent which informs us of the roughness and heterogeneities of the metal surface [24]; it can assume the following values: 1 (pure capacitance), 0.5 (Warburg diffusion), 0 (resistance) and -1 (inductance).

The impedance parameters of BM and HAZ immersed in blank and inhibited soil solution are listed in Table 5.

The double layer capacitance (C_{dl}) was calculated from (Eq. (7)) [66]:

$$C_{dl} = Y_0(\omega_{max})^{n-1} \quad (7)$$

Where: ω_{max} is the angular frequency at which the imaginary component of the impedance reaches its maximum value.

The Inhibition Efficiency (*IE* %) was calculated using the charge transfer resistance values (R_{ct}), by Eq. (8):

Table 5: EIS parameters of BM and HAZ in the blank NS3 soil solution and in presence of various concentrations of D2EHPA at 293 K.

Samples	C mM	R_S kΩ/cm^2	R_{ct} kΩ/cm^2	Y_0 S^n/mΩ.cm^2	n	χ^2 10^{-3}	C_{dl} mF/cm^2	IE%
	0	0.40	0.55	0.647	0.67	50	0.352	
BM	0.04	0.27	4.10	0.381	0.70	8.0	0.236	87.83
	0.08	0.27	8.21	0.226	0.71	5.7	0.152	93.93
	0.12	0.36	11.00	0.191	0.71	1.2	0.128	95.47
	0.16	0.35	25.49	0.150	0.71	8.1	0.108	98.04
	0	0.33	0.41	0.917	0.64	40	0.444	
HAZ	0.04	0.40	11.72	0.434	0.65	6.8	0.407	96.53
	0.08	0.39	16.06	0.361	0.65	4.02	0.362	97.47
	0.12	0.39	20.70	0.194	0.71	2.7	0.272	98.08
	0.16	0.38	30.36	0.196	0.71	8.9	0.168	98.66

$$IE\ (\%) = \frac{R_{ct(inh)} - R_{ct(0)}}{R_{ct(inh)}} \times 100 \qquad (8)$$

Where $R_{ct(inh)}$ and R_{ct} are the charge-transfer resistance values with and without inhibitor, respectively. Analysis of the results gathered in Table 5 reveals that the R_s values are almost constant, those of the charge transfer R_{ct} increased and are accompanied by a decrease in capacitance (C_{dl}) values as the concentration of D2EHPA increases. The highest value of R_{ct} corresponds to the maximum inhibition efficiency (98.04% for BM and 98.66% for HAZ) recorded at the maximum concentration of D2EHPA (0.16 mM), for both samples. This indicates that the adsorbed inhibitor molecules form a protective layer on the steel/solution interface [67]. It should be noted that in the case of HAZ, an inhibition efficiency greater than 95% was obtained regardless of the concentration of D2EHPA used. In addition, the decrease in the capacitance value with increasing inhibitor concentration may be caused by an increase in the thickness of the electrical double layer [68]. Indeed, according to the Helmholtz model (*Eq.* (9)), the decrease in the C_{dl} values indicates an increase in the double layer thickness (d), which can be attributed to the growth of a compact protective layer on the metal surface by the inhibitor adsorption [61].

$$C_{dl} = \varepsilon\, \varepsilon^{\circ}\, S/d \qquad (9)$$

Where d is the thickness of the film, ε° is the permittivity of the air, ε is the medium dielectric constant, and S represents the surface area of the working electrode.

As the concentration of D2EHPA increases its molecules are adsorbed by replacing the water molecules adsorbed onto the surface of BM and HAZ, inducing a thickening of the electrical double layer and therefore a decrease in the double layer capacity [23]. Moreover, the increase of n as concentration of D2EHPA increased reflects a decrease of roughness and heterogeneities of steel surface, resulting from the adsorption of D2EHPA molecules at the metal/solution interface.

These observations suggest that D2EHPA acts by adsorption on the active sites of BM and HAZ and thereby forms a thick film which isolates the surface of the two steels from the aggressiveness of the soil solution. The results obtained from EIS measurements are in good agreement with those determined from potentiodynamic polarization.

Adsorption isotherm at 293K

The inhibition mechanism is mainly attributed to the adsorption of the inhibitive molecules onto the metal surface, which represents the first step of this process [69]. Therefore, adsorption isotherms such as Langmuir, Frendlich, Temkin and Frumkin [70] are used to describe the adsorption process of inhibitors in order to understand the mechanism of the corrosion inhibition. Indeed, their determination can provide important information about the nature of metal-adsorbed inhibitor interactions [71]. In this study, among the previously mentioned isotherms, Langmuir isotherm was found to provide the best fit of our experimental data, which is modeled by (Eq. (10) [72]:

$$\frac{C_{inh}}{\theta} = \frac{1}{K_{ads}} + C_{inh} \qquad (10)$$

Where C_{inh} is the molar concentration of inhibitor, K_{ads} is the adsorption equilibrium constant and θ is the degree of surface coverage by inhibitor molecules and is calculated as follows:

$$\theta = \frac{IE\%}{100} \qquad (11)$$

The surface coverage (θ) values obtained from EIS method corresponding to different D2EHPA concentrations in the soil solution at 293 K, were used to deduce the best adsorption isotherm.

The plots of Cinh /θ vs C_{inh} are characterized by a straight line for BM and HAZ (Fig. 8) and their slope was close to 1, reflecting a significant interaction between D2EHPA molecules and steel surface, forming a monolayer of inhibitory film [73].

In addition, the correlation coefficient values (R^2) near to 1 suggested that D2EHPA adsorption onto the steel surface is

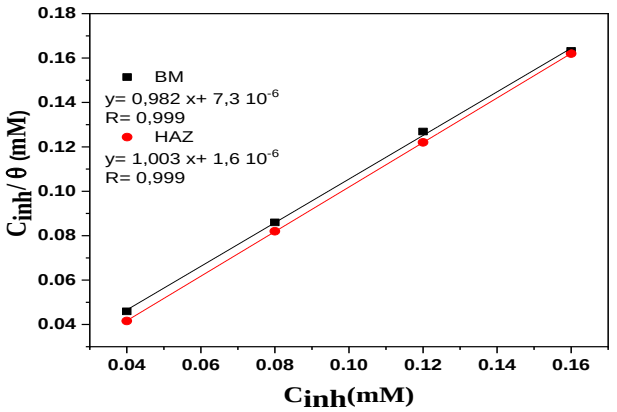

Fig. 8: Langmuir adsorption isotherm plots for BM and HAZ X60 using surface coverage calculated by EIS method.

modeled accurately by the Langmuir isotherm. This model implies that all the adsorption sites are equivalent and that there is no interaction among the adsorbed species [74].

Adsorption parameters deduced from Langmuir adsorption isotherms are recorded in Table 6. The value of the adsorption constant K_{ads} is related to the Gibbs free energy (ΔG°_{ads}) by (Eq. (12)):

$$\Delta G^{\circ}_{ads} = - RT \text{ Ln } (55.5 K_{ads}) \quad (12)$$

Where, R is the universal gas constant and T is the absolute temperature. The value of 55.5 is the concentration of water in the solution expressed in mol/dm [75].

The calculated values of ΔG°_{ads} for the two studied systems, BM and HAZ in the soil solution with D2EHPA, are shown in Table 6. The high values of K_{ads}, for BM ($1.345\ 10^5\ M^{-1}$) and HAZ ($6.268\ 10^5\ M^{-1}$), suggest a strong adsorption capacity of the inhibitor molecules on the metal surface [52]. It is commonly accepted that chemisorption, which is caused by charge sharing or electron transfer from the inhibitor molecules to the metal surface, occurs when ΔG°_{ads} values are around -40 kJ/mol or more negative [76]. Whereas if ΔG°_{ads} values are around or less negative than -20 kJ mol^{-1}, a second type of adsorption occurs *via* electrostatic interaction between the charged molecules and the charged metal surface; it is classified as physisorption. The value of ΔG°_{ads} for BM and HAZ are -38.553 kJ/mol and -42.302 kJ/mol, respectively. The large negative values of ΔG°_{ads} demonstrated that D2EHPA strongly adsorbs onto BM and HAZ surfaces and that the adsorption process is spontaneous, the same result has been reported by *M. Lebrini et al*. [56]. According to the obtained values of the adsorption standard free energy, we can postulate that a mechanism occurring during the

Table 6: Langmuir adsorption isotherm parameters obtained for BM and HAZ, using Θ deduced from EIS method at 293 K.

Samples	R^2	Slope	Intercept. 10^{-6}	K_{ads}. 10^4 M^{-1}	$-\Delta G^{\circ}_{ads}$ kJ/mol
BM	0.999	0.982	7.30	13.45	38.553
HAZ	0.999	1.003	1.60	62.68	42.302

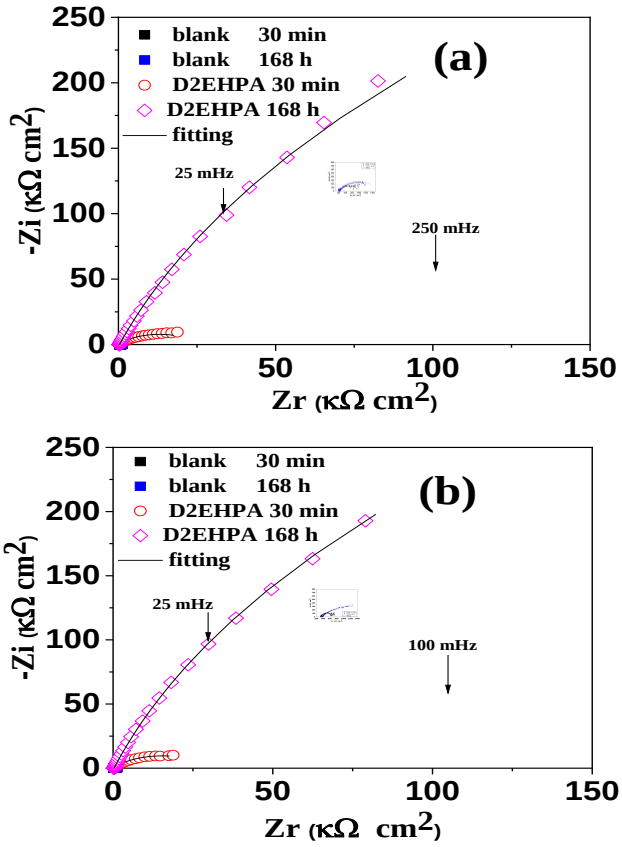

Fig. 9: Effect of immersion time on Nyquist plots for a) BM and b) HAZ and Bode plots of a') B M and b') HAZ in soil solution at different concentrations of the used inhibitor at 293 K

interactions between D2EHPA molecules and steel surface is based on chemical and physical interactions. Indeed, both physisorption and chemisorption contribute to the whole adsorption process [77], with a predominance of chemisorption as soon as the obtained values of ΔG°_{ads} are close to those characterizing a chemisorption process.

Effect of immersion time

The effect of immersion time (1800 s and 168 h) was carried out in the soil solution without D2EHPA and with its maximum concentration at room temperature, by impedance method, for both BM and HAZ materials (Fig. 9). In the absence of the inhibitor (insert in Fig. 9 (a, b)), the increasing of immersion time leads to an increase in the

Table 7: Effect of immersion time on EIS parameters for BM and HAZ in NS3 solution at 293 K without and with D2EHPA at 0.16 Mm.

Samples	*Time*	R_S kΩ/cm²	R_{ct} kΩ/cm²	Y_0 $S^n/\mu\Omega.cm^2$	n	C_{dl} µF/cm²	IE%
BM	30 min	0.40	0.55	647	0.67	353	/
	168 h	0.39	1.59	1105	0.53	687	/
	30 min	0.35	25.49	150	0.71	107.6	98.04
	168 h	0.34	1054.2	44.8	0.85	41.8	99.84
HAZ	30 min	0.33	0.41	917	0.64	444	/
	168 h	0.37	1.33	1674	0.48	881.5	/
	30 min	0.38	30.36	196	0.71	168.4	98.66
	168 h	0.30	1127.4	48.8	0.86	44.4	99.89

size of the capacitive loops. However, the shape of the EIS diagrams remains unchanged; indicating that the charge transfer still controls the corrosion process. The same phenomenon was observed in the presence of the inhibitor, but in a much more significant manner. In fact, the semi-circle diameter increased remarkably after 168 h of immersion for both samples. All of these observations suggest that on the one hand the corrosion products, formed after 168 h of immersion in the blank soil solution, accumulate on the steel surface, slowing down the dissolution process of BM and HAZ. On the other hand, the inhibitory effect of D2EHPA enhanced over time.

The equivalent circuit model used to fit the experimental impedance data of BM and HAZ in the soil solution without and with D2EHPA, at 1800 s and 168 h, is the same as that shown in Fig. 7. The deduced EIS parameters are given in Table 7.

In case of the blank soil solution, with increase of immersion time, both the R_{ct} and C_{dl} values increase. This could be related to a deposit of corrosion products onto the metal surface, induced by the metallic dissolution which increases the active surface of the studied samples. Indeed, *Bonnel et al*. [78] claimed that the C_{dl} values depend on the porosity and the conducting nature of the corrosion products. This is confirmed by the decrease over the time of the determined values of *n* for both steels in the blank solution. On the other hand, in the presence of D2EHPA, we note a clear increase of R_{ct} values and an appreciable decrease of C_{dl} values, after 168 h of immersion, for the two ferrous materials. As seen from Table 7 the inhibition efficiency values exceed 99% after 168 h of immersion of BM and HAZ in the soil solution in the presence of 0.16 mM of D2EHPA. This suggests a better protection provided by the phosphoric compound, by self-assembly of D2EHPA molecules, thus forming a stable layer at the metal surface during immersion time. This result could be correlated to the increase of the CPE exponent values *n* with immersion time.

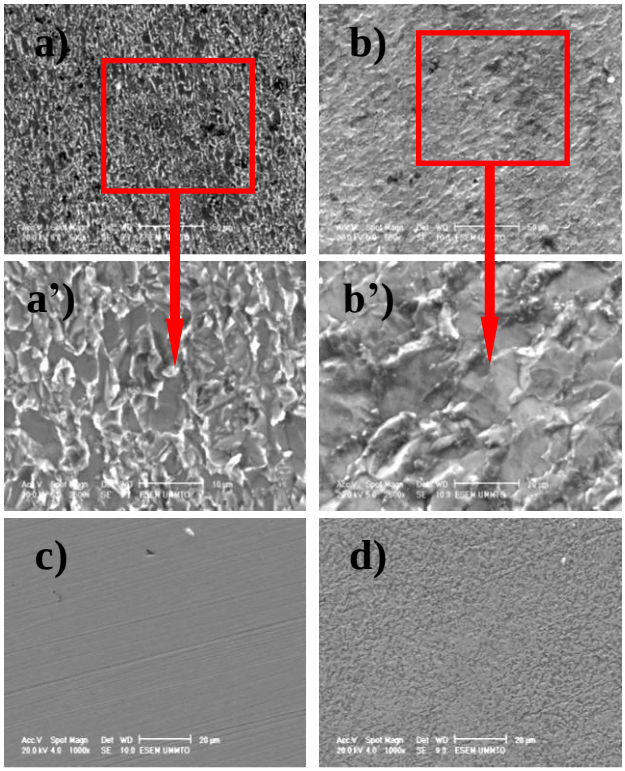

Fig. 10: SEM micrographs after 168 h of immersion in the blank soil solution for a) BM and b) HAZ, magnified image in uninhibited solution for a') BM and b') HAZ; in the presence of 0.16 mM of D2EHPA for c) BM and d) HAZ.

Surface Morphology

Scanning electron microscopy (SEM) was carried out to get more insight on the morphology of BM and HAZ surface, immersed for 168 h in NS3 solution at 293 K, with and without the studied inhibitor at 0.16 mM concentration (Fig. 10). This technique is commonly used to accurately observe the corroded and the protected metal surface [79,80]. Fig. 10 (a,b) demonstrates that in the absence of D2EHPA the surface of both samples is extremely damaged, due to the dissolution of the ferritic phase (anodic site). Indeed, the magnified micrographs (Fig. 10 (a', b')) show that the grain boundaries are preserved after the corrosive attack, which is preferentially localized on the ferrite grains for BM and HAZ. However, the surface degradation is more intense in the case of HAZ, due to the strong dissolution of the coarse grains of ferrite. Furthermore, the electrochemical

results showed that D2EHPA acts as anodic inhibitor by adsorbing on the anodic sites, represented by the ferritic phase, of BM and HAZ in the soil solution. Indeed, it is obvious that BM surface and HAZ surface (Fig. 10 (c, d)) are covered by a gray layer, in the presence of D2EHPA. However, in the case of BM surface it is remains remarkably homogeneous and smooth, because the anodic sites are represented by fine grains of ferrite, whereas, in the case of HAZ, they are depicted by coarse grains on which we clearly see that D2EHPA was adsorbed. Thus, we concluded that the D2EHPA deposit provides effective protection for BM and HAZ against the aggressiveness of the soil solution. These results are in agreement with the high inhibition efficiency values deduced from the electrochemical and thermodynamic studies.

DFT calculations

The theoretical chemistry methods are very useful in determining the molecular structure as well as elucidating the electronic structure and the reactivity of molecules. Therefore, it has become common to use quantum chemical calculations, such as density functional theory (DFT) calculations, in corrosion inhibitor studies [81].

The adsorption mechanism of D2EHPA can be studied using the theory of frontier molecular orbitals, HOMO (Highest Occupied Molecular Orbital) and LUMO (Lowest Unoccupied Molecular Orbital). Indeed, the effectiveness of the inhibitor molecule is significantly affected by its frontier molecular orbitals, because the donor-acceptor type interactions between inhibitor molecules and the metal surface are mediated by these peripheral molecular orbitals. According to the literature [82], the HOMO energy (E_{HOMO}) is associated with the electron donating ability of a molecule, whereas the LUMO energy indicates the capacity of a molecule to accept electrons. Thereby, the higher the E_{HOMO} values, the more likely it is that a molecule transfers electrons to the appropriate acceptor empty metal orbitals, and the lower the E_{LUMO} values, the easier it will be to transfer electrons from the full metal orbitals to a molecule [81]. As ΔE (E_{LUMO}-E_{HOMO}), named energy gap, corresponds to the energy required to remove an electron from the last occupied orbital, a low value of ΔE will induce strong adsorption of the inhibitor molecules and thus higher inhibition efficiency [83].

In the alkaline corrosive solution, D2EHPA may exist in the deprotonated form ($D2EHPA^{-}$) in equilibrium with its neutral form. According to *Lee P.C. et al*. [29], the negatively charged D2EHPA species dominate in the solution at pH higher of 4, thus, both D2EHPA and $D2EHPA^{-}$ are taken into account in the current study. Indeed, the studied soil solution, in the presence of the optimal concentration of D2EHPA has a pH value of 6.2.

The optimized structure, the frontier molecular orbitals, and Molecular Electrostatic Potential (MEP) of D2EHPA and the deprotonated D2EHPA are illustrated in Fig.11.

The location of frontier molecular orbitals may be used to predict the adsorption centers of the inhibitor molecule. Analysis of the Fig. 11 shows that the HOMO orbitals of the neutral D2EHPA are mainly distributed on the whole molecule, except on certain atoms. On the other hand, the LUMO orbitals are mostly localized around a phosphoric group and the carbon atoms which are directly linked to it.

However, in the case of $D2EHPA^{-}$, it can be seen that the HOMO and LUMO orbitals are well localized on the oxygen atoms of the phosphate group.

The energy gap $\Delta E_{|HOMO-LUMO|}$ is an important molecular descriptor of chemical stability, meaning that a low value of $\Delta E_{|HOMO-LUMO|}$ denotes a highly reactive molecule, suggesting that the electron density of the molecule can be easily changed, its resistance to charge transfer being smaller. The energy gap (ΔE) of the deprotonated molecule shown in Table 8 is lower than that of the neutral molecule; this indicates a higher tendency of the deprotonated compound to form chemical bonds with the metal. This is confirmed by the E_{HOMO} and E_{LUMO} values of $D2EHPA^{-}$.

The electrophilicity index (ω) is an important parameter that indicates the tendency of a molecule to accept electrons [45]. According to the literature, a molecule having a low electrophilicity index would have good corrosion inhibitory properties [84]. In the present work, the deprotonated inhibitor ($DEHPA^{-}$) has the lowest electrophilicity index, therefore, it can be stated that the anionic molecule would be more effective against corrosion than the neutral molecule, in the studied soil solution.

The number of the transferred electrons (ΔN), representing the electron-donating ability of a molecule, was also calculated. As mentioned by *Lukovits et al*. [82], for ΔN values less than 3.6, the inhibition efficiency increases with the increase of electron-donating ability of a molecule. It is also stated that if $\Delta N > 0$, the electron transfer takes place favorably from the molecule to the metal, and if $\Delta N < 0$, the transfer is from the metal to the molecule. As seen in

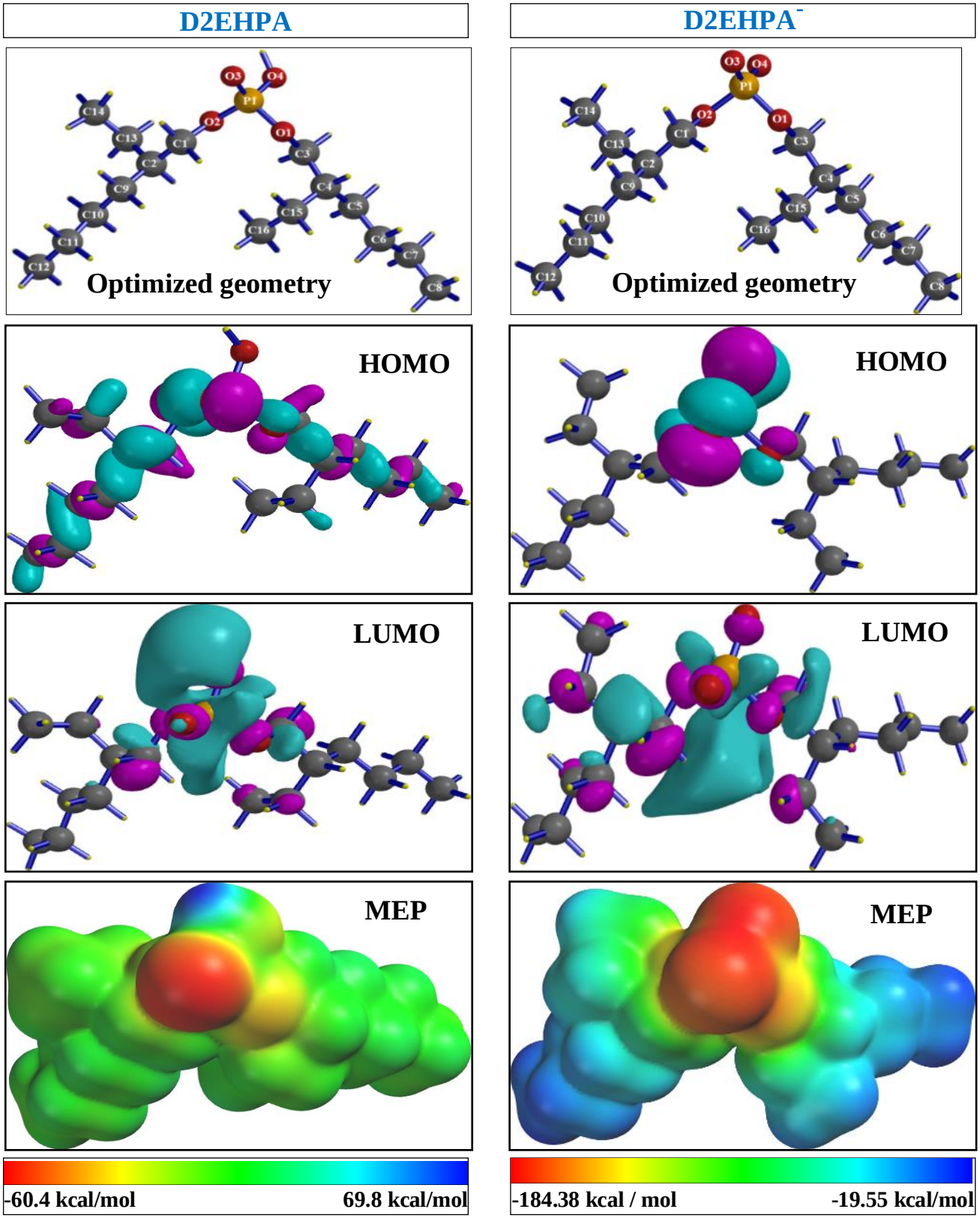

Fig. 11: The optimized structure, the HOMO orbitals, the LUMO orbitals and Molecular Electrostatic Potential (MEP) of D2EHPA and deprotonated D2EHPA

Table 8: Quantum chemical parameters of D2EHPA and D2EHPA$^-$at the DFT/6-31G** Levels.

Inhibitor	E_{HOMO} (eV)	E_{LUMO} (eV)	ΔE (gap) (eV)	μ (Debye)	χ (eV)	η (eV)	ω (eV)	ε	ΔN
D2EHPA	-8.03	1.13	9.16	4.36	3.45	4.58	1.29	0.77	0.38
D2EHPA$^-$	-6.05	1.48	7.53	16.93	2.28	3.76	0.69	1.45	0.63

Table 9: Values of the Mulliken charges for D2EHPA and D2EHPA $^-$ at the DFT/6-31G** Levels.

D2EHPA		D2EHPA$^-$	
Atom	Charge	Atom	Charge
P1	1.41	P1	0.958
O1	-0.531	O1	-0.572
O2	-0.520	O2	-0.568
O3	-0.646	O3	-0.731
O4	-0.540	O4	-0.738
C1	0.035	C1	0.051
C2	-0.080	C2	-0.046
C3	0.026	C3	0.042
C4	-0.079	C4	-0.040
C5	-0.175	C5	-0.175
C6	-0.170	C6	-0.168
C7	-0.175	C7	-0.169
C8	-0.319	C8	-0.315
C9	-0.179	C9	-0.172
C10	-0.167	C10	-0.160
C11	-0.176	C11	-0.169
C12	-0.318	C12	-0.314
C13	-0.179	C13	-0.173
C14	-0.328	C14	-0.327
C15	-0.187	C15	-0.176
C16	-0.334	C16	-0.311

Table 8, the calculated Δ*N* values of the selected molecules are positive and less than 3.6, pointing out to transfer of electrons from the molecules to the metal surface, meaning the strong and stable adsorption of the two D2EHPA forms on steel surface in the simulated solution.

The relatively high value of the dipole moments (μ) of the deprotonated molecules indicates their high polarity, inducing powerful electrostatic interactions with the metal surface. As a corollary, these dipolar interactions have led to the strong adsorption of these molecules. Furthermore, the values of (μ) related to D2EHPA and D2EHPA$^-$ were greater than that of the water molecule (μ_{H2O} =1.85 D). This result is another support for the preferential adsorption of the two forms of D2EHPA molecules onto the metal surface over that of water molecules [85].

Molecular Electrostatic Potential (MEP) illustrated in Fig. 11 is a visual method that allows us to distinguish the location of the electron density. In these maps, different colors are observed, where the red represents the zone with the negative potential of MEP, associated with reactive electrophilic sites, the blue color is adapted to the zone with the positive potential and represents the suitable center of the nucleophilic attacks [48]. The red colored region in the neutral molecule is concentrated mainly on the O (3) oxygen atom, while the blue region is located around hydrogen of the OH group.

However, in the case of D2EHPA$^-$ represented in Fig. 11, the positive charge is obviously concentrated on the carbon atoms C (8) and C (12) and the negative charge is localized on both oxygen atoms O (3) and O (4) illustrated by the red color region. The main advantage of this presentation is to separate electron density and electrostatic potential surfaces with clarity and compactness. The principal disadvantage is that it provides information only about the contact surface and does not reveal how far electron-rich and electron-poor areas extend beyond the surface.

The existence in the inhibitor molecule of several atoms with high negative partial charge determines the occurrence of a higher number of donor-acceptor interactions and therefore a better adsorption of D2EHPA at the metal/solution interface.

The Mulliken charge values for D2EHPA and D2EHPA$^-$, listed in Table 9, show the existence of several atoms with a high tendency to donate electrons to the metal surface and these atoms are: O (1), O (2), O (3), and O (4). Therefore, it may be supposed the chemical interactions of D2EHPA with metal surface are possible by these adsorption centers, which is why it can be affirmed that it supports the hypothesis of a chemical adsorption. However, we remark that the charges of the oxygen atoms of D2EHPA$^-$ are higher than that of the neutral form, indicating a stronger adsorption of the anionic species on the metal surface.

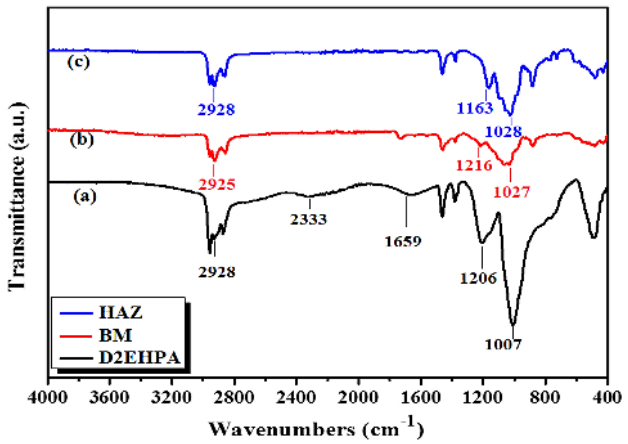

Fig. 12: FT-IR spectra for a) pure D2EHPA and adsorbed layer on b) BM and c) HAZ surface after 168 h of immersion in soil solution with 0.16 mM of D2EHPA.

FT-IR spectroscopy

FT-IR study for pure D2EHPA and the adsorbed layer of D2EHPA, on the BM and the HAZ surface (Fig. 12), was carried out in order to evaluate the protective ability of the D2EHPA layer and also to localize the functional groups of D2EHPA responsible for the binding on the two steels surface. The FT-IR spectra of free D2EHPA and D2EHPA adsorbed on the steel surface, after 168 h of immersion in the soil solution with the optimal concentration of the inhibitor, are illustrated in Fig. 12. Analysis of FT-IR spectrum (Fig. 12 (a)) shows that the most characteristic of stretching frequencies for D2EHPA are P–O–H (2550-2750=2333 cm^{-1}), P=O (1206.31 cm^{-1}), P-O-C (1007.1 cm^{-1}), C-C (486 cm^{-1}), and C-H at 2928, 95 cm^{-1} attributed to stretching for alkanes. We also note that D2EHPA displays a broad band at 1659.88 cm^{-1} corresponding to P-O-H group deformation [86]. The principal bands observed in the FT-IR spectra of the adsorbed layer on BM (Fig. 12 (b)) and HAZ (Fig. 12 (c)) surface closely correspond to those appearing in the D2EHPA spectrum. It should be noted that the C-H peak remains unchanged in the spectra of pure D2EHPA and of the adsorbed layer on the two samples surface. However, we observe shifts of the molecular vibrations to higher or lower wave-numbers and a decrease in the peak's intensity of the P-O-C, P=O and P-O-H bands. This suggests that D2EHPA has bonded with Fe^{2+} which confirms the involvements of these centers in the adsorption of D2EHPA, forming Fe^{2+}–D2EHPA complexes on the surface of the studied steels [87].

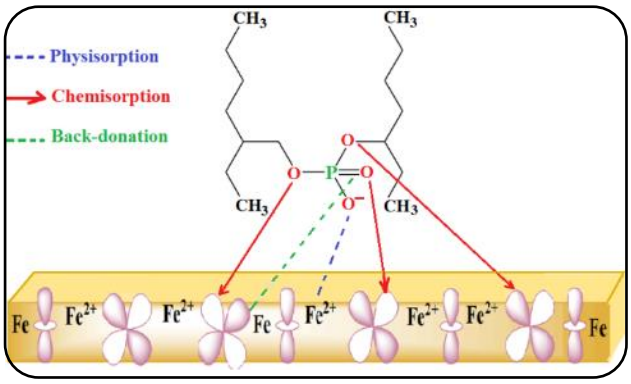

Fig. 13: The proposed adsorption mechanism of $D2EHPA^-$ onto BM and HAZ surface

Adsorption mechanism of D2EHPA

Based on the obtained results during this study, namely the experimental and theoretical results, it is obvious that D2EHPA is an effective inhibitor which acts by adsorption on the surface of BM and HAZ in the soil solution. This adsorption can be represented as a substitutional adsorption process between the D2EHPA molecules in the aqueous solution and the adsorbed water molecules on the metallic surface [88].

Indeed, the ΔG°_{ads} and K_{ads} values suggest that the inhibitor is strongly adsorbed at the metal/solution interface, in the case of both studied systems. This result is confirmed by the SEM micrographs which reveal an unaltered surface of the two steels after 168 h of their immersion in the soil solution in the presence of D2EHPA at 0.16 mM. The FT-IR spectra also prove the presence of the principal functional groups of D2EHPA in the adsorbed layer [89].

On the other hand, in the studied alkaline soil solution, D2EHPA may exist in the deprotonated form ($D2EHPA^-$) in equilibrium with its neutral form. Thus, the quantum chemical study has been carried out for the D2EHPA and its anionic form; all the calculated quantum descriptors suggest that it is the latter which is more reactive and apt to adsorb on the metal surface than the neutral form. This reactivity occurs through the oxygen atoms of the phosphate group. Fig. 13 illustrates the proposed adsorption mechanism of $D2EHPA^-$ to highlight the various interactions between the inhibitive molecules and the steel surface.

We can then state that the deprotonated form was adsorbed in two stages: the first one corresponds to an electrostatic attraction between the deprotonated oxygen O (4) and the ferrous ions, present at the metal/solution interface, and the second step consists of a transfer of the lone-

pair electrons from the oxygen O (1), the oxygen O (2), and the oxygen O (3) of the phosphoryl group (P=O), to the vacant d-orbital of iron surface atoms. This refers to donor-acceptor interactions ensuring the chemical adsorption. A retro-donation mechanism can also explain the metal-D2EHPA interactions; it consists of the transfer of electrons from the ferrous atoms to the empty π^* of the inhibitor molecule [81].

CONCLUSION

This study examined the electrochemical corrosion behaviour of BM and HAZ of API L5 X60 pipeline steel in a simulated soil solution (NS3) at 293 K, and the ability of Di-(2-ethylhexyl) phosphoric acid (D2EHPA) to protect the two systems against soil corrosion. The experiments were conducted using several techniques such as open circuit potential (OCP), potentiodynamic polarization, impedance (EIS) and surface analysis. Then, they were supplemented by DFT calculations. It was shown that HAZ is less corrosion resistant than BM in the soil solution, due to its coarse microstructure. The inhibition of the corrosion of BM and HAZ was provided by D2EHPA. It was found to be an efficient anodic type corrosion inhibitor for HAZ and BM in the soil solution, and its inhibition efficiency increases with the increase of its concentration. The adsorption of D2EHPA at the interface steel/solution fit well with the model of the Langmuir adsorption isotherm; it occurs through physisorption and chemisorption with predominance of chemisorption. An inhibition efficiency of D2EHPA, exceeding 99%, was recorded for both samples after 168 hours of immersion in the inhibitive solution at the concentration of 0.16 mM in inhibitor. Based on the electrochemical measurements, SEM micrographs and FT-IR spectra it is concluded that D2EHPA is a very efficient corrosion inhibitor for soil corrosion of BM and HAZ. Besides, DFT descriptors demonstrated that the deprotonated form of D2EHPA is more reactive than its neutral form. Our work will be completed by the effect of temperature, in order to determine the activation parameters (energy, enthalpy and entropy) and to get more insight in the mechanism of D2EHPA adsorption onto the steel surface. The influence of pH will be also examined, as it is an essential parameter in the soil corrosion.

FUNDING

This research was supported by DGRSDT-MESRS (Direction Générale de la Recherche Scientifique et du Développement Technologique - Ministère de l'Enseignement Supérieur et de la Recherche Scientifique).

Received: May. 29, 2022 ; Accepted: Aug. 22, 2022

References

[1] Ren C.Q., Xian N., Wang X., Liu L., Zheng Y.P., Susceptibility of Welded X80 Pipeline Steel to Corrosion in Simulated Soil Solution, *Corros. Eng. Sci. Tech.*, **47:** 441-445 (2012).

[2] Cui Y, Lundin C.D., Evaluation of Initial Corrosion Location in E316L Austenitic Stainless Steel Weld Metals, *Mater. Lett.*, **59:** 1542–1546 (2005).

[3] Azevedo C. R. F., Failure Analysis of a Crude Oil Pipeline, *Eng. Fail. Anal.*, **14:** 978– 994 (2007).

[4] Zhang C., Cheng Y. F., Corrosion of Welded X100 Pipeline Steel in a Near-Neutral pH Solution, *J. Mater. Eng. Perform.*, **19:** 834–840 (2010).

[5] Alves V.A., Brett C.M.A., Cavaleiro A., Influence of Heat Treatment on The Corrosion of High Speed Steel, *J. Appl. Electrochem*, **31:** 65–72 (2001).

[6] Zhang G.A., Cheng Y.F., Micro-Electrochemical Characterization of Corrosion of Welded X70 Pipeline Steel in Near-Neutral pH Solution, *Corros. Sci.*, **51:** 1714–1724 (2009).

[7] Chaves I.A., Melchers R.E., Pitting Corrosion in Pipeline Steel Weld Zones, Corros. *Sci.*, **53:** 4026–4032 (2011).

[8] Mohammadi F., Eliyan F.F., Alfantazi A., Corrosion of Simulated Weld HAZ of API X-80 Pipeline Steel, *Corros. Sci*., **63:** 323–333 (2012).

[9] Durr C.L., Beavers J.A., "Techniques for Assessment of Soil Corrosivity", *Corros. NACE Intern.*, (1998).

[10] Noor A.E., Al-Moubaraki H.A., Influence of Soil Moisture Content on the Corrosion Behavior of X60 Steel in Different Soils, *Arab. J. Sci. Eng., 2014*, **39:** 5421-5435 (2014).

[11] Lins V.F.C., Ferreira M.L.M., Saliba P.A., Corrosion Resistance of API X52 Carbon Steel in Soil Environment, *J. Mater Res. Tech.*, **1:** 161–166 (2012).

[12] Lim K.S., Nordin Y., Siti Rabeah O., Siti Nor F., Norhazilan M.N., The Relationship between Soil Resistivity and Corrosion Growthin Tropical Region, *J. Corros. Sci. Eng.*, **54:** 1-11 (2013).

[13] Shwethambika P., Ishwara Bhat J., Matured Theobroma Cocoa Pod Extracts as Green Inhibitor for Acid Corrosion of Aluminium, *Iran. J. Chem. Chem. Eng. (IJCCE)*, **40(3):** 906-919 (2021)

[14] Kartsonakis I.A., Stamatogianni P., Karaxi E.K., Charitidis C.A., Comparative Study on the Corrosion Inhibitive Effect of 2-Mecraptobenzothiazole and Na2HPO4 on Industrial Conveying API 5L X42 Pipeline Steel, *Appl. Sci.*, **10:** 290-327 (2020).

[15] Kalyn T., Poberezhny L., Popovych P., Rudiak Y., Korol O., Poberezhna L., Evaluation of the Green Inhibitor Effect on the Corrosion of Pipeline Steel in NS4 Medium, *Proc. Stru. Integr*., **36:** 313–317 (2022).

[16] Tristijanto H., Ilman M.O., Iswanto P.T., Corrosion Inhibition of Welded of X – 52 Steel Pipelines by Sodium Molybdate in 3.5% NaCl Solution, *Egypt. J. Pet.*, **29:** 155-162 (2020).

[17] Slimane M., Kellou F., Kellou-Tairi S., Electrostatic Adsorption of Hexamethylenetetramine as a Corrosion Inhibitor for FeTi1.88C2.35 Cast Iron in Electrolytic Acid Solution, *Res. Chem. Intermed*., **41:** 8571–8590 (2015).

[18] Noorollahy Bastam N., Hafizi Atabak H. R., Atabaki F., Radvar M., Jahangiri S., Electrochemical Measurements for the Corrosion Inhibition of Mild Steel in 0.5 M HCl using Poly(Epichlorohydrin) Derivatives, *Iran. J. Chem. Chem. Eng.*, **39(4):** 113-125 (2020).

[19] Bashir S., Sharma V., Lgaz H., Chung I.M., Singh A., Kumar A., The Inhibition Action of Analgin on the Corrosion of Mild Steel in Acidic Medium: A Combined Theoretical and Experimental Approach, *J. Mol. Liq*., **263:** 454-462 (2018).

[20] Akbarzade K., Danaee I., Nyquist Plots Prediction using Neural Networks in Corrosion Inhibition of Steel by Schiff base, *Iran. J. Chem. Chem. Eng.*, **37(3):** 135-143 (2018)

[21] Bashir S., Lgaz H., Chung I.M., Kumar A., Potential of Venlafaxine in the Inhibition of Mild Steel Corrosion In HCl: Insights from Experimental and Computational Studies, *Chem. Pap*., **73(9):** 2255-2264 (2019).

[22] Jafari H., Mohsenifar F., Sayin K., Effect of Alkyl Chain Length on Adsorption Behavior and Corrosion Inhibition of Imidazoline Inhibitors, *Iran. J. Chem. Chem. Eng.*, **37(5):** 85–103 (2018).

[23] Bhuvaneswari T.K, Jeyaprabha C., Arulmathi P., Corrosion Inhibition of Mild Steel in Hydrochloric Acid by Leaves Extract of Tephrosia Purpure, *J. Adhes. Sci. Technol.*, **34(22):** 2424-2447 (2020).

[24] Vazquez A.E., Resendiz L.A.L et al., Corrosion Inhibition Assessment on API 5L X70 Steel by Preussomerin G Immersed in Saline and Saline Acetic, *J. Adhes. Sci. Technol*., **35(8):** 873-899 (2020).

[25] Aljebory R.Z.J., Al-Saadi F.A.J., Husseini M.D.M., Drugs as Corrosion Inhibitors for the Environment–A Review, *Al-Kufa University Journal for Biology*., **5:** 100227 (2022).

[26] Wranglen G., "An Introduction to Corrosion and Protection of Metals", *Chapman and Hall, New York* (1985).

[27] Hluchan V., Wheeler B L., Hackerman N., Amino Acids as Corrosion Inhibitors in Hydrochloric Solutions, *Mater. Corros.*, **39:** 512-517 (1988).

[28] Karthik B.B., Selvakumar P., Thangavelu C., Phosphonic Acids Used as Corrosion Inhibitors-A review, *Asian. J. Chem.*, **24:** 3303-3308 (2012).

[29] Lee P.C., Li C.W., Chen J'Y., et al., Dissolution of D2EHPA in Liquid-Liquid Extraction Process: Implication on Metal Removal and Organic Content of the Treated Water, *Water Res.*, **45:** 5953-5958 (2011).

[30] Elmi S., Foroughi M.M., Dehdab M., Shahidi Z.M., Computational Evaluation of Corrosion Inhibition of Four Quinoline Derivatives on Carbon Steel in Aqueous Phase, *Iran. J. Chem. Chem. Eng*, **38(1):** 185-200 (2019).

[31] Obi-Egbedi N.O., Obot I.B., El-Khaiary M.I., et al., Computational Simulation and Statistical Analysis on the Relationship between Corrosion Inhibition Efficiency and Molecular Structure of some Phenanthroline Derivatives on Mild Steel Surface, *Int. J. Electrochem. Sci.*, **6:** 5649-5675 (2011).

[32] Idir B., Kellou-Kerkouche F., Experimental and Theoretical Studies on Corrosion Inhibition Performance of Phenanthroline for Cast Iron in Acid Solution, *J. Electrochem. Sci. Technol.*, **9:** 260-275 (2018).

[33] Parkins R.N., Blanchard Jr W.K., Delanty B.S., Transgranular Stress Corrosion Cracking of High-Pressure Pipelines in Contact with Solutions of Near Neutral pH, *Corrosion*, **50:** 394–408 (1994).

[34] Becke A.D., Density-Functional Exchange-Energy Approximation with Correct Asymptotic Behavior, *Phys. Rev.*, **38:** 3098-3100 (1988).

[35] Becke A.D., Density-Functional Thermochemistry. III. The Role of Exact Exchange, *J. Chem. Phys.*, **98:** 5648-5652 (1993)

[36] Becke A.D., A New Mixing of Hartree–Fock and Local Density-Functional Theories, *J. Chem. Phys.*, **98:** 1372-1377 (1993).

[37] Lee C., Yang W., Parr R.G., Development of the Colle-Salvetti Correlation-Energy formula into a Functional of the Electron Density, *Phys. Rev. B. Condens Matter*, **37:** 785- 789 (1988).

[38] Miehlich B., Savin A., Stolt H., Preuss H., Results Obtained with the Correlation Energy Density Functionals of Becke and Lee, Yang and Parr, *Chem. Phys. Lett.*, **157:** 200-206 (1989).

[39] Petersson G.A., Al-Laham M.A., A Complete Basis Set Model Chemistry. II. Open-Shell Systems and the Total Energies of the First-Row Atoms, *J. Chem. Phys.*, **94:** 6081-6090 (1991).

[40] Petersson G.A, Bennett A., Tensfeldt T.G., Al-Laham M.A., Shirley W.A., Mantzaris J., A Complete Basis Set Model Chemistry. I. The Total Energies of Closed-Shell Atoms and Hydrides of the First-Row Elements, *J. Chem. Phys.*, **89:** 2193-2218 (1988).

[41] Frisch M.J., Trucks G.W., Et al., Gaussian 03. Revision A.1. Gaussian Inc, *Pittsburgh. P. A* (2003).

[42] Fuentealba P., Cardenas C., Density Functional Theory of Chemical Reactivity, *Chem. Modell.*, **11:** 151-174 (2014).

[43] Geerlings P., De Proft F., Langenaeker W., Conceptual Density Functional Theory, *Chem Rev.*, **103:** 1793-1874 (2003).

[44] Parr R.G., Pearson R.G., Absolute Hardness, Companion Parameter to Absolute Electronegativity, *J. Am. Chem.Soc.*, **105:** 7512-7516 (1983).

[45] Parr R.G, Szentpaly L., Liu S., Electrophilicity Index, *J. Am. Chem. Soc.*, **121:** 1922- 1924 (1999).

[46] Chattaraj P.K., Sarkar U., Roy D.R., Electrophilicity Index, *Chem. Rev.*, **106:** 2065– 2091 (2006).

[47] Pearson R.G., Absolute Electronegativity and Hardness: Application to Inorganic Chemistry, *Inorg. Chem.*, **27:** 734-740 (1988).

[48] Madkour L.H., Kaya S., Kaya C., Guo L., Quantum Calculations Molecular Dynamics Simulation and Experimental Studies of Using Some Azo Dys as Corrosion Inhibitors for Iron, *J. Tai. Inst. Chem. Eng.*, **68:** 461-480 (2016).

[49] Ashby M. F., "Choix des Matériaux en Concéption Mécanique. Dunod (3°Ed.)", *Techniques et Ingénierie*, (2012).

[50] De Sena R.A., Bastos I.N., Platt G.M., Theoretical and Experimental Aspects of the Corrosivity of Simulated Soil Solutions, *ISRN Chemical Engineering*, *International Scholarly Research Notices*, **2012:** 103715 (2012).

[51] Bueno A.H., Gomes J.A., Environmentally Induced Cracking of API Grade Steel in Near-Neutral pH Soil, *J. Braz. Soc. Mech. Sci. Eng.*, **31(2):** 97-104 (2009).

[52] Wahdan M.H., Hermas A. A., Morad M. S., Corrosion Inhibition of Carbon-steels by Propargyltriphenylphosphonium Bromide in H_2SO_4 Solution, *Mater. Chem. Phys.*, **76:** 111–118 (2002).

[53] Cleary H. J., Greene N. D., Corrosion Properties of Iron and Steel, *Corros. Sci.*, **7(2):** *821*-831 (1967)

[54] Felhősi I., Keresztes Z., Kármán F. H., Mohai M., Bertóti I., Kálmán E., Effects of Bivalent Cations on Corrosion Inhibition of Steel by 1-Hydroxyethane-1,1-Diphosphonic Acid, *J. Electrochem. Soc.*, **146(3):** 961-969 (1999).

[55] Kálmán E., Várhegyi B., et al., Corrosion Inhibition by 1-Hydroxy-Ethane-1, 1-Diphosphonic Acid: An Electrochemical Impedance Spectroscopy Study, *J. Electrochem Soc.*, **141(12):** 3357-3360 (1994).

[56] Lebrini M., Robert F., Vezin H., Roos C., Electrochemical and Quantum Chemical Studies of Some Indole Derivatives as Corrosion Inhibitors for C38 Steel in Molar Hydrochloric Acid, *Corros. Sci.*, **52:** 3367-3376 (2010).

[57] Xu B., Ji Y., Zhang X., et al., Experimental and Theoretical Studies on the Corrosion Inhibition Performance of 4-Amino-N, N, Di-(2-Pyridylmethyl)-Aniline on Mild Steel in Hydrochloric Acid, *RSC. Adv.*, **5:** 56049-56059 (2015).

[58] Mameri S., Boughrara D., Chopart J., Kadri A., Electrochemical Corrosion Behavior of API 5L X52 Pipeline Steel in Soil Environment, *Anal. Bioanal. Electrochem.*, **13:** 239-263 (2021)

[59] Bommersbach P., Dumont C.A., Millet J.P., Normand B., Hydrodynamic Effect on the Behaviour of a Corrosion Inhibitor Film: Characterization by Electrochemical Impedance Spectroscopy**,** *Electrochim. Acta*, **51(19):** 4011-4018 (2006).

[60] Tan B., Zhang S., Cao X., Fu A., Guo L., Marzouki R., Li W., Insight into the Anti-Corrosion Performance of Two Food Flavors as Eco-Friendly and Ultra-High Performance Inhibitors for Copper in Sulfuric Acid Medium, *J. Colloid. Interface. Sci.*, **609:** 838–851 (2022).

[61] Brug Guo L., Tan J., Kaya S., Leng S., Li Q., Zhang F., Multidimensional Insights Into the Corrosion Inhibition of 3,3-Dithiodipropionic Acid on Q235 Steel in H_2SO_4 Medium: A Combined Experimental and in Silico Science, investigation, *J. Colloid. Interface. Sci.*, **570:** 116–124 (2020).

[62] Brug G.J., Van Den Eeden A.L.G., Sluyters-Rehbach M., et al., The Analysis of Electrode Impedances Complicated by the Presence of a Constant, *J. Electroanal. Chem. Interfacial. Electrochem*, **176:** 275–295 (1984).

[63] Xu B., Yang W., Liu Y., Et al., Experimental and Theoretical Evaluation of Two Piyridinecarboxaldehyde Thiosemicarbasone Compounds as Corrosion Inhibitors for Mild Steel in Hydrochloric Acid Solution, *Corros. Sci.*, **78:** 260-268 (2014).

[64] Khan G., Newaz K.M.S., Basirun W.J., et al., Application of Natural Product Extracts as Green Inhibitors for Metals and Alloys in Acid Pickling Processes, *Inter. J. Electrochem. Sci.*, **10(8):** 6120-6134 (2015).

[65] Macdonald J.R., Impedance Spectroscopy and its use in Analyzing the Steady-State AC Response of Solid and Liquid Electrolytes, *J. Electroanal Chem. Interfacial Electrochem*, **223:** 25-50 (1987).

[66] Hsu C.H., Mansfeld F., Technical note: Concerning the Conversion of the Constant Phase Element Parameter Y0 into a Capacitance, *Corrosion-Houston Tx*, **57(9):** 747-748 (2001).

[67] Abd- El Rehim S.S., Ibrahim M.A.M., Khalid K.F., The Inhibition of 4-(2'-amino-5'-methylphenylazo) Antipyrine on Corrosion of Mild Steel in HCl Solution, *Mater. Chem. Phys.*, **70:** 268-273 (2001).

[68] Khaled K.F., Molecular Simulation, Quantum Chemical Calculations and Electrochemical Studies for Inhibition of Mild Steel by Triazoles, *Electrochim. Acta*, **53(9):** 3484- 3492 (2008).

[69] Asan A., Kabasakaloglu M., Isiklan M., Kilic Z., Corrosion Inhibition of Brass in Presence of Terdentate Ligands in Chloride Solution, *Corros. Sci.*, **47:** 1534-1544 (2005).

[70] Kadhim A., Al-Okbi K., Jamil D.M., et al., Experimental and Theoretical Studies of Benzoxazines Corrosion Inhibitors, *Results. Phys.*, **7:** 4013–4019 (2017).

[71] Ashassi-Sorkhabi H., Chabani B., Aligholipour B., Seifzadeh D., The Effect of Some Shiff Bases on the Corrosion of Aluminum in Hydrochloric Acid Solution, *Appl. Surf. Sci.*, **252:** 4039-4047 (2006).

[72] Musa A.Y., Kadhum A.A.H., Mohamad A.B., Rahoma A.A.B., Mesmari H., Electrochemical and Quantum Chemical Calculations on 4, 4-dimethyloxazolidine-2- thione as Inhibitor for Mild Steel Corrosion in Hydrochloric Acid, *J. Mol. Struct.*, **969:** 233-237 (2010).

[73] Badiea A.M, Mohana K.N., Effect of Temperature and Fluid Velocity on Corrosion Mechanism of Low Carbon Steel in Presence of 2-Hydrazino-4,7-Dimethylbenzothiazole in Industrial Water Medium, *Corros. Sci.*, **51:** 2231-2241 (2009).

[74] Solomon M.M., Umoren S.A., Udosoro I.I., Udoh A.P., Inhibitive and Adsorption Behavior of Carboxymethyl Cellulose on MS Corrosion in Sulphuric Acid Solution, *Corros. Sci.*, **52(4):** 1317-1325 (2010).

[75] Fuchs-Godec R., Dolecek V., A Effect of Sodium Dodecylsufate on the Corrosion of Copper in Sulphuric Acid Media, *Colloids. Surf. A.*, **244:** 73–76 (2004).

[76] Zhang Q., Hua Y., Corrosion Inhibition of Aluminum in Hydrochloric Acid Solution by Alkylimidazolium Ionic Liquids, *Mater. Chem. Phys.*, **119:** 57–64 (2010).

[77] Khaled K.F., Electrochemical Investigation and Modeling of Corrosion Inhibition of Aluminum in Molar Nitric Acid Using some Sulphur-Containing Amines, *Corros. Sci.*, **52:** 2905–2916 (2010).

[78] Bonnel A., Dabosi F., Deslouis C., Dupart M., Keddam M., Trabolet B., Corrosion Study of a Carbon Steel in Neutral Chloride Solutions by Impedance Techniques, *J. Electrochem. Soc.*, **130:** 753-761 (1983).

[79] Ashassi-Sorkhabi H., Ghalebsaz-Jeddi N., Effect of Ultrasonically Induced Cavitation on Inhibition Behavior of Polyethylene Glycol on Carbon Steel Corrosion, *Ultrason. Sonochem.*, **13(2):** 180-188 (2006).

[80] Lopez D.A., Schreiner W.H., De Sanchez S.R., Simson S.N., The Influence of Carbon Steel Microstructure on Corrosion Layers. An XPS and SEM Characterization, *Appl. Surf. Sci.*, **207(1-4):** 69-85 (2003).

[81] Chaouiki A., Lgaz H., Salghi R., et al., Inhibitory Effect of a new Isoniazid Derivative as an Effective Inhibitor for Mild Steel Corrosion in 1.0 M HCl: Combined Experimental and Computational Study, *Res. Chem. Intermed.*, **46:** 2919-2950 (2020).

[82] Lukovits I., Kalman E., Zucchi F., Corrosion Inhibitors-Correlation Between Electronic Structure and Efficiency, *Corrosion*, **57(1):** 3-8 (2001).

[83] Issa R.M., Awad M.K., Atlam F.M., Quantum Chemical Studies on the Inhibition of Corrosion of Copper Surface by Substituted Uracils, *App. Surf. Sci.*, **255(5):** 2433- 2441 (2008).

[84] El-Din M.R.N., Khamis E.A., Corrosion Inhibition Efficiency, Electrochemical and Quantum Chemical Studies of some New Nonionic Surfactants for Carbon Steel in Acidic Media, *J. Surfact. Deterg*, **17(4):** 795- 805 (2014).

[85] Hegazy M.A., Novel Cationic Surfactant Based on Triazole as a Corrosion Inhibitor for Carbon Steel in Phosphoric Acid Produced by Dihydrate Wet Process, *J. Mol. Liq.*, **208:** 227-236 (2015).

[86] Nakamoto K., Ferraro J.R., Mason G.W., Vibrational Spectra and Normal Coordinate Treatment of Bis(2-ethylhexyl) Hydrogen Phosphate, *Applied Spectroscopy*, **23:** 521-527 (1969).

[87] Li X.H, Deng S.D., Fu H., Inhibition by Jasminum Nudiflorum Lindl Leaves Extract of the Corrosion of Cold Rolled Steel in Hydrochloric Acid Solution, *J. Appl. Electrochem*, **40:** 1641–1649 (2010).

[88] Rajeswari V., Kesavan D., Gopiramanb M., Viswanathamurthi P., Physicochemical Studies of Glucose, Gellan Gum, and Hydroxypropyl Cellulose-Inhibition of Cast Iron Corrosion, *Carbohydr. Polym*, **95:** 288- 294 (2013).

[89] Xometl O.O., Álvarez E.A., et al., Synthesis and Corrosion Inhibition Mechanism of Ammonium-Based Ionic Liquids on API 5L X60 Steel in Sulfuric Acid Solution, *J. Adhes. Sci. Tech.*, (2017).